LETTERS

Contact force measurements and stress-induced anisotropy in granular materials

T. S. Majmudar[1] & R. P. Behringer[1]

Interparticle forces in granular media form an inhomogeneous distribution of filamentary force chains. Understanding such forces and their spatial correlations, specifically in response to forces at the system boundaries[1,2], represents a fundamental goal of granular mechanics. The problem is of relevance to civil engineering, geophysics and physics[3–5], being important for the understanding of jamming, shear-induced yielding and mechanical response. Here we report measurements of the normal and tangential grain-scale forces inside a two-dimensional system of photoelastic disks that are subject to pure shear and isotropic compression. Various statistical measures show the underlying differences between these two stress states. These differences appear in the distributions of normal forces (which are more rounded for compression than shear), although not in the distributions of tangential forces (which are exponential in both cases). Sheared systems show anisotropy in the distributions of both the contact network and the contact forces. Anisotropy also occurs in the spatial correlations of forces, which provide a quantitative replacement for the idea of force chains. Sheared systems have long-range correlations in the direction of force chains, whereas isotropically compressed systems have short-range correlations regardless of the direction.

Under the action of external stresses, grains in dry granular materials form an inhomogeneous contact network, which carries most of the external load by way of force chains. The resultant network is different for shearing than for isotropic compression and is history-dependent owing to friction. Previous experiments[6–8] have reported an exponential tail for the distribution of contact force magnitudes. This tail can be successfully predicted by many models[9–11] with radically different mathematical structures and microscopic assumptions. Testing the validity of these models requires that the predicted force distributions be verified by measurements of full vectorial contact forces in the bulk of the sample. It is also important to find other distinguishing signatures characterizing the nature of force chain networks under different boundary conditions—an important goal of the present work.

In the following experiments, we visualize internal stresses in each grain and by solving the full inverse photoelastic problem[12,13] for each disk, we obtain normal and tangential force components for each contact between disks. We use this microscopic contact force information to investigate differences in the distributions of contact forces, and the force chain structure, arising from two different types of loads: pure shear and isotropic compression. We find that forces have distinctive angular distributions and spatial correlations depending on the macroscopic preparation. In particular, forces have long-range correlations in the direction of force chains for sheared systems, but are correlated over a much shorter range, regardless of direction, for isotropically compressed systems.

Our experimental system is a two-dimensional (2D) array of approximately 2,500 bidisperse photoelastic (birefringent under strain) disks subjected to pure shear and isotropic compression. Figure 1 shows a diagram of the experimental set-up and some typical images; details of the set-up and the experimental procedure are described in Fig. 1 legend. Although previous approaches[14–17] have obtained contact forces using photoelastic techniques, they were neither automated nor suitable for a large enough number of

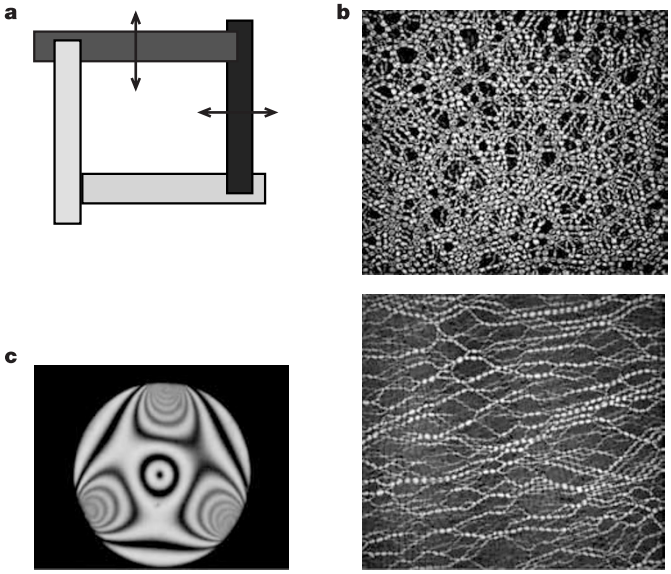

Figure 1 | Experimental set-up and representative data. **a**, Schematic diagram of the biaxial test cell. The biaxial test apparatus rests horizontally on a sheet of Plexiglas and is used to impart pure shear and isotropic compression. Motorized linear slides move two walls of the biaxial cell precisely and independently with a velocity of 0.024 cm s^{-1}. The system is illuminated from below and a high-resolution camera captures digital images from above. Each image captures roughly 250 particles located around the centre of the cell, roughly 10% of the total number of particles. The system is imaged through crossed circular polarizers. For each type of load, incremental deformations are applied in a quasi-static manner, beginning with a stress-free state. The sheared states are created by compressing in one direction and expanding by an equal amount in the other direction, with strains ($\varepsilon_{xx} = \varepsilon_{yy} = |\Delta L/L|$) ranging from 0 to 0.042. L (~40 cm) is the initial system length in the x or y direction. Isotropically compressed states are created by compressing in both directions with strains ranging from 0 to 0.016. The particles used in the experiment are either 0.8 cm or 0.9 cm in diameter and 0.6 cm in height, with a Young's modulus of 4 MPa and a friction coefficient of 0.8. The number ratio of small to large disks is 4:1. **b**, Typical system size images for an isotropically compressed state (top) and a sheared state (bottom). **c**, An example of the observed stress pattern for a single disk at the resolution (~0.01 cm per pixel) used in these studies.

[1]Department of Physics & Center for Nonlinear and Complex Systems, Duke University, Durham, North Carolina, 27708-0305, USA.

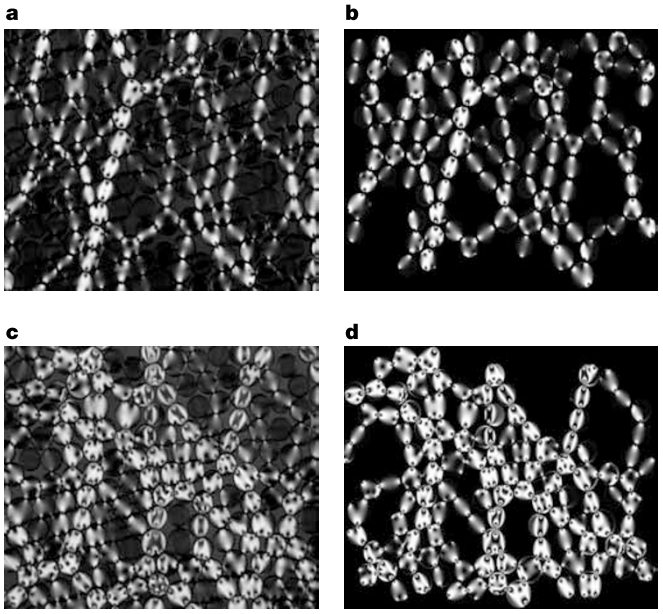

Figure 2 | Comparison of experimental images (a, c) and computed images (b, d). Top pair, a low-force sheared state. Bottom pair, a high-stress isotropically compressed state. Very weak forces are not resolved owing to a force threshold involved in the algorithm. Forces lower than 10% of the mean force are not computed.

particles to generate statistical information. Measurements of contact forces in our method are performed in a completely automated fashion for all disks except those at the boundary of the image.

Our algorithm for extracting contact forces (T.S.M. and R.P.B., manuscript in preparation) involves fitting the observed photoelastic pattern inside each disk to the plane elasticity solution[18] for the stresses inside a disk, treating the force components as fitting parameters. In effect we solve the 2D isotropic elasticity equations for each disk, assuming a perfect line contact between three-dimensional (3D) cylinders. As long as the deformations are not too large, as is the case in our experiments, the 2D solution is a good approximation. As the experimental image is a highly nonlinear function of the contact forces with the possibility of multiple solutions, we perform a nonlinear least-squares fit[19] using about 500 data points for each disk. The best-fit parameter values are our measured contact forces.

For each realization, we compare the image computed using the best-fit contact forces and the original experimental image. Figure 2 shows two such realizations. The computed images (Fig. 2b, d) agree well with the experimental images (Fig. 2a, c) in terms of capturing the broad features of force chains. The error estimates found by calibration and by computing the average difference of pairs of forces at each contact are around 10% for low forces and 5% for mean-to-high forces. The agreement between the observed stress field inside each disk and the computed stress field validates the use of the 2D approximation. The data presented below (Figs 3 and 4) are obtained from five realizations for each stress state. We use the contact forces obtained by the procedure outlined above to investigate the distributions of contact forces and the anisotropy induced by external loads.

Figure 3 shows the distributions of the normal force, the tangential force and the ratio of tangential to normal force, for a sheared system and an isotropically compressed system. The normal and the tangential forces are normalized by the mean normal force. The normal force distribution for the sheared system (Fig. 3a) has a peak around the mean, a roughly exponential tail and a dip towards zero for forces lower than the mean. In contrast, for isotropically compressed systems, the normal force distribution (Fig. 3c) dips towards zero for forces below the mean, is broad around the mean, and decays faster for large forces compared to the sheared system. The tangential force distributions have a nearly exponential tail for forces larger than the mean for both the sheared (Fig. 3a) and the isotropically compressed system (Fig. 3c). The mean tangential forces are an order of magnitude smaller than the mean normal forces: a feature responsible for a smaller range of maximum tangential forces.

In order to investigate the role of friction in the system, we study the distribution of the variable $S = |F_t|/\mu F_n$, where μ is the static friction coefficient, F_t is the tangential force, and F_n is the normal force. The variable S gives information about how far away a contact is from the Coulomb failure criterion. If a contact is at the Coulomb failure criterion, $S = 1$. Figure 3b and d show the distributions of S for the sheared and the isotropically compressed system, respectively. For both types of loading conditions, the distribution of S shows that most of the contacts are much below the Coulomb failure condition.

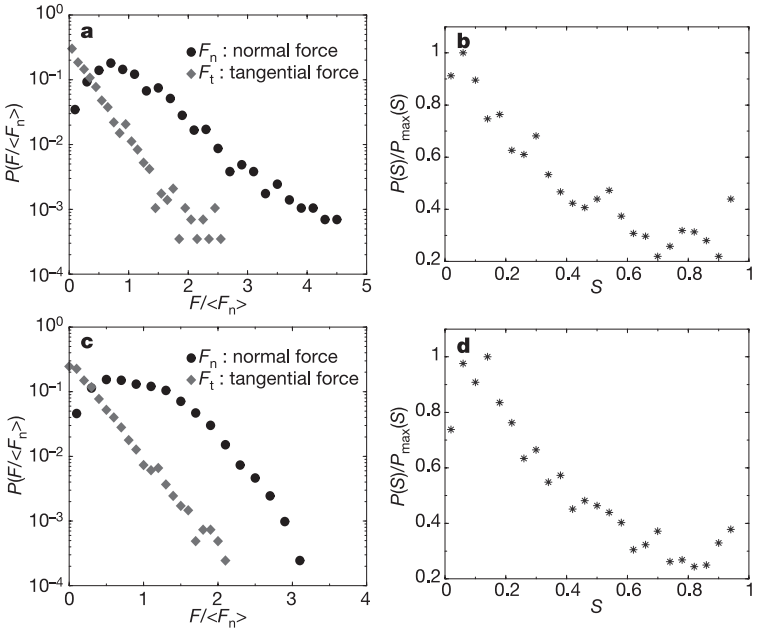

Figure 3 | Probability distributions of the normal forces, the tangential forces, and the mobilized friction, for the sheared and the isotropically compressed systems. The deformation ($\varepsilon_{xx} = \varepsilon_{yy} = |\Delta L/L|$) for isotropically compressed and sheared systems is 0.016 and 0.042, respectively. In **a** and **c**, the forces are normalized by the mean normal force, $\langle F_n \rangle$. **a**, Probability distributions of the normal (F_n) and the tangential (F_t) forces for the sheared system on a semi-log scale. **b**, Probability distribution of $S = |F_t|/\mu F_n$ for the sheared system, normalized by its maximum value, $P_{max}(S)$. **c**, Probability distributions of the normal and the tangential forces for the isotropically compressed system on a semi-log scale. **d**, Probability distribution of $S = |F_t|/\mu F_n$ for the isotropically compressed system, normalized by its maximum value.

Numerical simulations of 3D granular systems in a silo geometry[20] report similar results for the distributions of the normal forces and the tangential forces in sheared systems. The distributions of the variable S (also called the mobilized friction) in the interior of the system reported in ref. 21 are qualitatively similar to our results for the sheared systems. The similarity in the distributions of the mobilized friction for the sheared and the isotropically compressed systems could be due to the fact that our sheared system is well below the shear yield limit and that our distributions are obtained from regions far away from the walls.

Our next focus of investigation is the shear-induced anisotropy. The anisotropy induced by an external load has two distinct effects; one, a purely geometric effect, is to introduce anisotropy in the contact network, and the other, a mechanical effect, is to develop an anisotropic force chain network and alter the stress distribution in the system. In order to investigate the geometric anisotropy, we study the distribution of contact angles for contacts carrying forces larger than the mean force. The sheared system (Fig. 4a) shows a strongly anisotropic distribution, with a large number of contacts aligned along the direction of the majority of force chains and a small number of contacts aligned in the direction perpendicular to it. In contrast, the isotropically compressed system exhibits a distribution with a six-fold symmetry (Fig. 4b), indicating that the contacts are distributed evenly along these directions. A simple measure characterizing the mechanical anisotropy is the angular variation of the mean normal force as shown in Fig. 4c and d, for the sheared and the isotropically compressed system, respectively. For the sheared system, the mean normal force shows a periodic variation with peaks roughly in the direction of force chains. The variation can be adequately described by a second-order Fourier expansion (Fig. 4c), a result consistent with previous studies[22,23]. In contrast, for the isotropically compressed system, the mean normal force is distributed randomly around an average value (Fig. 4d).

A more quantitative characterization of the force chain structure can be obtained by computing the 2D spatial correlation function of the magnitude of the forces on the particles. Here, the idea is to provide a well-defined quantitative measure to replace the rather vaguely defined notion of a force chain. Force correlation functions, in combination with force and angular distributions, provide an additional tool for discriminating among competing theories. Specifically, we computed $\langle F(\mathbf{x})\ F(\mathbf{x}+\mathbf{r})\rangle$, where $F(\mathbf{x})$ is the sum of the magnitudes of the contact forces on a particle, $\mathbf{x}$ gives the position vector of the point under consideration, and $\langle\ldots\rangle$ implies an average over $\mathbf{x}$. Because we want to study the variation of this correlation in different directions, we do not average over angles. Thus, the correlation function gives spatial correlation between forces separated by a distance $\mathbf{r}$ in different directions. Figure 4e and f show the 2D correlation functions for the sheared system and the isotropically compressed system, respectively. The inset in each case shows a greyscale representation of the 2D correlation function. For the sheared system, the 2D correlation image (Fig. 4e, inset) reveals that the force correlations are much larger and of much longer range in the direction of the long force chains. Figure 4e, which depicts the variation of correlation function with distance in the

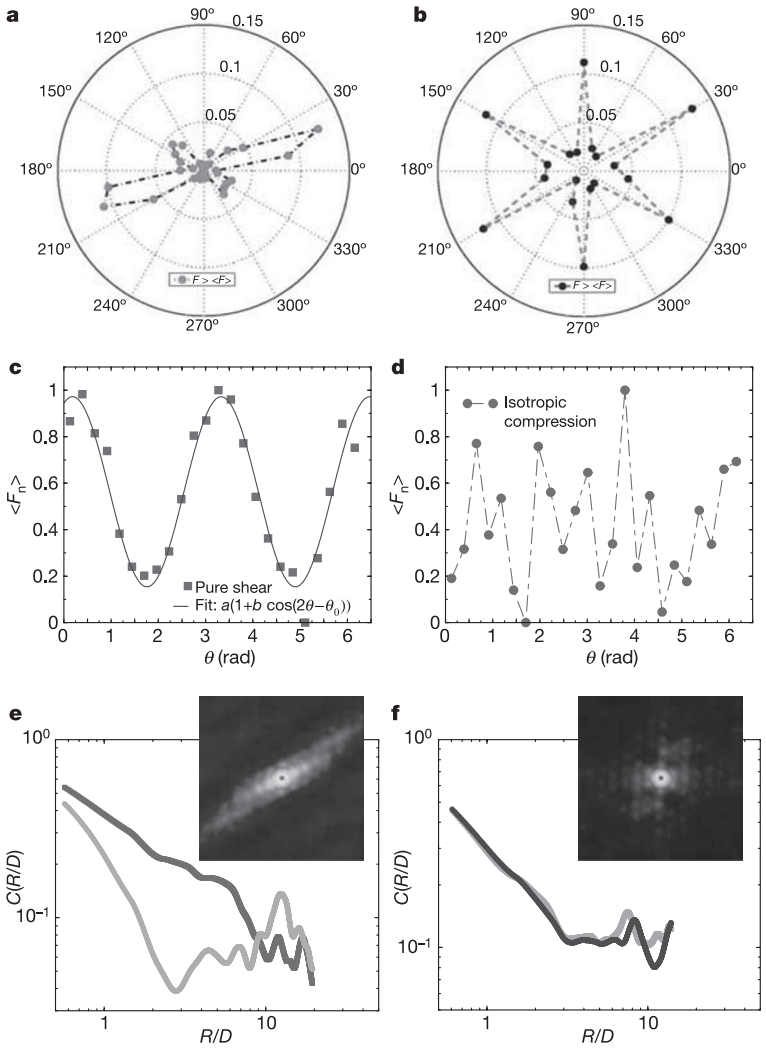

Figure 4 | Contact orientation, variation of the mean force and spatial correlations for the sheared and the isotropically compressed systems. The mean co-ordination numbers for the sheared system and the isotropically compressed system are 3.1 and 3.7, respectively. The deformations for each type of loads are the same as in Fig. 3. **a**, **b**, The distribution of contact angles of contacts carrying forces larger than the mean, for the sheared and the isotropically compressed system, respectively. **c**, **d**, The angular variation of the mean normal force, normalized by the maximum of the mean normal force (denoted only as $\langle F_n\rangle$ for clarity), for the sheared and the isotropically compressed system, respectively. Starting from the centre of the image, the image is divided into 24 angular bins of 15° each and the average normal force in each bin is plotted against the mean value of that bin. The angle (θ) in radians is measured with respect to the horizontal axis. The parameters of the fit in **c** are $a = 0.563$, $b = 0.727$ and $\theta_0 = 0.374$. The parameter a gives the mean force, b is a measure of anisotropy of the mean force, and θ_0 gives the direction in which the mean force is maximum. **e**, Spatial correlations for the sheared system in the direction of force chains and perpendicular to it. **f**, Spatial correlations for the isotropically compressed system in the same two directions used for the sheared system. The insets of **e** and **f** show the greyscale representations of the 2D correlations. The darker regions correspond to low correlation values, and brighter regions to high correlation values. The computations are performed in Fourier space, as the image sizes are large (1,600 × 1,152). The plots are on a log–log scale with distance R normalized by the average diameter D of the disks.

direction of, and perpendicular to, the force chains, indicates that the spatial correlations in the force chain direction persist for up to ~15 particle diameters, whereas in the perpendicular direction they fall to background values within a couple of particle diameters. The correlation range in the direction of force chains is comparable to half the image size, which is 15 particle diameters in length. This length is also the Nyquist cut-off frequency of the Fourier method for computing the force correlation function in our computed images. The above data suggest the interesting possibility that the spatial force correlation may in fact be of a power-law type in the direction of long force chains for large system sizes.

In complete contrast to sheared systems, the isotropically compressed system has nearly uniform force correlation in all directions (Fig. 4f, inset). This behaviour is confirmed by examining the spatial correlation functions for the isotropically compressed system (Fig. 4f). For ease of comparison, the correlations are shown for the same two directions used for the sheared case. The correlation functions drop to background values in both directions after two particle diameters. Thus, no preferred direction is found in the isotropically compressed system, whereas in the sheared system the boundary stress creates an anisotropic stress state characterized by long force chains aligned in a specific direction. Our results strongly indicate that sheared systems exhibit not only geometric but also mechanical anisotropy, and that force correlations serve as an additional distinguishing signature characterizing stress-induced anisotropy in granular systems. The rather long range of correlations in the force chain direction is important for understanding the approach to continuum behaviour.

The observations reported here open up a new regime of comparison between theoretical models and experiments. One of the earliest computations of interparticle contact forces comes from numerical experiments[11], which are contact dynamics simulations of rigid, frictional particles under biaxial shear. Although the boundary conditions of the simulations and our experiments are not identical, these simulations seem to be the closest match to our experiments. As our current experimental resolution does not allow us to measure very small forces, we restrict our comparison to forces higher than the mean. In qualitative agreement with our data for the sheared systems, the simulations obtain an exponential tail for forces larger than the mean for the distributions of both the normal and the tangential forces.

Two recent models, which study the force distributions in 2D systems of frictionless particles under isotropic compression and shear, are also relevant for the present data. A force ensemble approach by Snoeijer *et al.*[23] assumes equal a priori probability for all force networks consistent with force balance constraints on each particle. In this model, the distribution of the magnitude of the force, $P(f)$, has a peak around the mean force, a finite value at $f = 0$, and a tail decaying faster than an exponential for compressed systems. For sheared systems, the model has an exponential regime for normal forces up to three times larger than the mean (J. Snoeijer, personal communication). A new lattice model[24] considers triangular lattices with force balance constraints on each node, which allows isotropic and anisotropic force chain networks. The lattice model prediction for the distribution of normal forces is an exponential tail for the sheared systems and a faster than exponential decay of the tail for compressed systems. The predictions of both models for sheared and isotropically compressed systems are in qualitative agreement with the present data. The absence of friction in both these models precludes a comparison of the distributions of tangential forces.

Looking towards the future, we are now in a position to address a variety of important issues, such as the nature of the jamming transition and the response function of a granular system. These issues are vital for gaining a deeper understanding of the macroscopic behaviour of granular systems from microscopic observations. Future goals will be the extension of these studies to yet larger systems and smaller forces.

Received 23 February; accepted 6 May 2005.

1. Geng, J. *et al.* Footprints in sand: The response of a granular material to local perturbations. *Phys. Rev. Lett.* **87,** 035506 (2001).
2. Reydellet, G. & Clément, E. Green's function probe of a static granular piling. *Phys. Rev. Lett.* **86,** 3308–3311 (2001).
3. Behringer, R. P. & Jenkins, J. T. (eds) *Powders and Grains 97* (Balkema, Rotterdam, 1997).
4. Nedderman, R. M. *Statics and Kinematics of Granular Materials* (Cambridge Univ. Press, Cambridge, UK, 1992).
5. Jaeger, H. M., Nagel, S. R. & Behringer, R. P. Granular solids, liquids, and gases. *Rev. Mod. Phys.* **68,** 1259–1273 (1996).
6. Meuth, D. M., Jaeger, H. M. & Nagel, S. R. Force distribution in a granular medium. *Phys. Rev. E* **57,** 3164–3169 (1998).
7. Løvoll, G., Måløy, K. J. & Flekkøy, E. G. Force measurements on static granular materials. *Phys. Rev. E* **60,** 5872–5878 (1999).
8. Tsoungui, O., Vallet, D. & Charmet, J. Use of contact area trace to study the force distributions inside 2D granular systems. *Granular Matter* **1,** 65–69 (1998).
9. Goldenberg, C. & Goldhirsch, I. Small and large scale granular statics. *Granular Matter* **6,** 87–97 (2003).
10. Snoeijer, J. H., van Hecke, M., Somfai, E. & van Saarloos, W. Force and weight distributions in granular media: Effects of contact geometry. *Phys. Rev. E* **67,** 030302(R) (2004).
11. Radjai, F., Wolf, D. E., Jean, M., Roux, S. & Moreau, J. in *Powders & Grains 97* (eds Behringer, R. P. & Jenkins, J. T.) 211–214 (Balkema, Rotterdam, 1997).
12. Frocht, M. M. *Photoelasticity* Vol. 1 (Wiley & Sons, New York, 1941).
13. Frocht, M. M. *Photoelasticity* Vol. 2 (Wiley & Sons, New York, 1948).
14. Drescher, A. & De-Josselin-de-Jong, G. Photoelastic verification of a mechanical model for the flow of a granular material. *J. Mech. Phys. Solids* **20,** 337–351 (1972).
15. Durelli, A. J. & Wu, D. Use of coefficients of influence to solve some inverse problems in plane elasticity. *J. Appl. Mech.* **50,** 288–296 (1983).
16. Shukla, A. & Nigam, H. A numerical-experimental analysis of the contact stress problem. *J. Strain Anal.* **20,** 241–245 (1985).
17. Paikowsky, S. G., DiRocco, K. J. & Xi, F. in *2nd Int. Conf. on Discrete Element Methods (DEM)* (eds Williams, J. R. & Mustoe, G. W.) 449–461 (IESL Publications, MIT, Boston, 1993).
18. Landau, L. *Theory of Elasticity* (Pergamon, New York, 1959).
19. Press, W. H., Teukolsky, H. A., Vetterling, W. T. & Flannery, B. P. *Numerical Recipes in C: The Art of Scientific Computing* (Cambridge Univ. Press, Cambridge, UK, 1992).
20. Landry, J. W., Grest, G. S., Silbert, L. E. & Plimpton, S. J. Confined granular packings: Structure, stress, and forces. *Phys. Rev. E* **67,** 041303 (2003).
21. Silbert, L. E., Grest, G. S. & Landry, J. W. Statistics of the contact network in frictional and frictionless granular packings. *Phys. Rev. E* **66,** 061303 (2002).
22. Cambou, B., Dubujet, Ph. & Nouguier-Lehon, C. Anisotropy in granular materials at different scales. *Mech. Mater.* **36,** 1185–1194 (2004).
23. Snoeijer, J. H., Vlugt, T. J. H., van Hecke, M. & van Saarloos, W. Force network ensemble: A new approach to static granular matter. *Phys. Rev. Lett.* **92,** 054302 (2004).
24. Tighe, B. P., Socolar, J. E. S., Schaeffer, D. G., Mitchener, W. G. & Huber, M. L. Force distributions in a triangular lattice of rigid bars. Preprint at ⟨http://arXiv.org/cond-mat/0505003⟩ (2005).

Acknowledgements This work was supported by NSF DMR, NSF DMS, and NASA. We thank J. Snoeijer and collaborators, J. Socolar and B. Tighe for providing their data and for discussions. We thank H. Phatnani for critical reading of the manuscript.

Author Information Reprints and permissions information is available at npg.nature.com/reprintsandpermissions. The authors declare no competing financial interests. Correspondence and requests for materials should be addressed to R.P.B. (bob@phy.duke.edu).